Award Number: W81XWH-12-1-0097

TITLE: "Targeting Alpha5 Beta1 Integrin to Prevent Metastatic Breast Cancer Cell Invasion: PhScN Target Site Definition and Plasma Stability"

PRINCIPAL INVESTIGATOR: Philip Andrews

CONTRACTING ORGANIZATION: The Regents of the University of Michigan
Ann Arbor, MI 48109

REPORT DATE: November 2015

TYPE OF REPORT: Final

PREPARED FOR: U.S. Army Medical Research and Materiel Command
Fort Detrick, Maryland 21702-5012

REPORT DOCUMENTATION PAGE

Form Approved
OMB No. 0704-0188

1. REPORT DATE	2. REPORT TYPE	3. DATES COVERED
November 2015	Final	1Sep2012 - 31Aug2015

4. TITLE AND SUBTITLE
Targeting Alpha5 Beta1 Integrin to Prevent Metastatic Breast Cancer Cell Invasion: PhScN Target Site Definition and Plasma Stability

5a. CONTRACT NUMBER

5b. GRANT NUMBER
W81XWH-12-1-0097

5c. PROGRAM ELEMENT NUMBER

6. AUTHOR(S)
Philip Andrews

Email: andrewsp@umich.edu

5d. PROJECT NUMBER

5e. TASK NUMBER

5f. WORK UNIT NUMBER

7. PERFORMING ORGANIZATION NAME(S) AND ADDRESS(ES)
The Regents of the University of Michigan
Ann Arbor, MI 48109

8. PERFORMING ORGANIZATION REPORT NUMBER

9. SPONSORING / MONITORING AGENCY NAME(S) AND ADDRESS(ES)
U.S. Army Medical Research and Materiel Command
Fort Detrick, Maryland 21702-5012

10. SPONSOR/MONITOR'S ACRONYM(S)

11. SPONSOR/MONITOR'S REPORT NUMBER(S)

12. DISTRIBUTION / AVAILABILITY STATEMENT
Approved for Public Release; Distribution Unlimited

13. SUPPLEMENTARY NOTES

14. ABSTRACT
We proposed to test PHSCN and PhScN derivatives with modifications of the N– or C–termini, and/or cysteine side chain to determine the initial spatial constraints of the binding pocket of the ligand to its target site. This will aid in the selection of crosslinking agents, modifications, tag additions and strategies for determination of the target site(s) performed in Aim 2 and lay the foundation for determining the structure-activity relationships (SARS) of these inhibitors with the target.

15. SUBJECT TERMS- none listed

16. SECURITY CLASSIFICATION OF:			17. LIMITATION OF ABSTRACT	18. NUMBER OF PAGES	19a. NAME OF RESPONSIBLE PERSON
a. REPORT	b. ABSTRACT	c. THIS PAGE			USAMRMC
U	U	U	UU	24	19b. TELEPHONE NUMBER *(include area code)*

Table of Contents

INTRODUCTION: It has been suggested that PHSCN inhibits metastatic invasion by forming a covalent, disulfide bond with a cysteine residue on the beta1 (β1) subunit of alpha5 beta1 (α5β1) integrin[1]. However, these studies were performed with purified α5β1 integrin, which also produces evidence of covalent bond formation with the α5 subunit (tandem mass spectroscopy data not shown). Hence, the specificity of the reported interaction between PHSCN and the β1 subunit[1] is suspect. Moreover, the cysteine–rich β1 subunit can heterodimerize with 12 distinct alpha integrin subunits[2], forming integrins that function in many pathways. In contrast, the α5 subunit interacts uniquely with the β1 subunit[2] to induce invasion and support adhesion[3-5]; thus it is a much more desirable target. Our research tested definitively the hypothesis that both PHSCN and PhScN peptides inhibit α5β1 integrin fibronectin receptor–mediated invasion through noncovalent interaction with α5β1 receptors of SUM149PT and MDA-MB-231 metastatic human breast cancer cells, and laid the foundation for detailed structure–activity relationship (SAR) studies for both peptides as inhibitors of α5β1–mediated metastatic breast cancer invasion.
Objective/Hypothesis: The data, summarized below in Figures 1–6 and in Tables1–4, and presented in our submitted manuscript, *Therapeutic Inhibition of Breast Cancer Bone Metastasis Progression and Lung Colonization: Breaking the Vicious Cycle by Targeting α5β1 Integrin*, by Hongren Yao, Donna M. Veine, and Donna L. Livant, show that the invasion–inhibitory potencies of the S–acetylated and the S–methylated PHSCN peptide derivatives are increased by 10,000–fold and 1,000,000–fold, respectively, relative to PHSCN. The PhScN peptide is also highly potent: our results show that it is 100,000–fold more potent than PHSCN at blocking α5β1–mediated invasion. Furthermore, inclusion of a total of 8 (acetylated) Ac-PhScNGGK sequences on a polylysine dendrimer, as we did to increase the potency of the PHSCN sequence[12,13], results in an increase of invasion–inhibitory potency of 10^{11} to 10^{12}–fold. Our data, summarized in Figures 1-6 and in Tables 1–4 below, and presented in the manuscript, *Therapeutic Inhibition of Breast Cancer Bone Metastasis Progression and Lung Colonization: Breaking the Vicious Cycle by Targeting α5β1 Integriin*, show that the actual invasion–inhibitory interaction of PHSCN with α5β1 integrin involves a noncovalent interaction with the target site, which is promoted by including D–isomers of histidine and cysteine in the PhScN peptide. Thus, covalent, disulfide bond formation with α5β1 integrin is actually a side reaction that *decreases* potency. Because mammalian proteins do not contain D–amino acids, endoproteinses evolved to cleave between L–amino acids only. Since PhScN does not contain 2 linked L–amino acids, it cannot be degraded by endoproteases, usually present at high levels in tumors and increasing with malignancy[6-8]. Thus, in addition to promoting noncovalent interaction with its α5β1 integrin target, the inclusion of D–amino acids at alternate positions likely results in increased PhScN potency as a result of preventing endoproteolytic degradation. Finally, the *in vivo* lung extravasation and colonization data, as well as the bone colony progression data presented in Figures 3, 4, and 5, show that systemic PhScN therapy is a highly effective, well–tolerated systemic mono–therapy for reducing lung colonization and metastasis progression, as well as intratibial progression by metastatic breast cancer. The figures and tables presented in this annual report are listed below.
Figure 1. Hill–Slope plots of increased invasion–inhibitory potency of Ac-PhScN-NH_2, Ac-PhScNGGK-MAP, and the cysteine–modified, methylated (Me) or acetylated (O-Ac) peptides for MDA-MB-231 cells.
Figure 2. Hill–Slope plots of invasion inhibition by biotinylated derivatives of PHSCN and PhScN for MDA-MB-231 cells, induced by FBS, K_d binding assays for biotinylated Ac-PHSCNGGK-Bio (CN-Bio) and Ac-PhScNGGK-Bio (cN-Bio) peptides with suspended MDA-MB-231 cells, and competition binding to suspended MDA-MB-231 cells of Ac-PHSCNGGK-Bio and varying concentrations of unlabeled Ac-PhScN-NH_2.
Figure 3. Increased extravasation inhibition by Ac-PhScN-NH_2 peptide or Ac-PhScNGGK-MAP dendrimer prebinding, relative to Ac-PHSCN-NH_2.
Figure 4. increased inhibition of lung colonization by Ac-PhScN-NH_2 prebinding, relative to Ac-PHSCN-NH_2.
Figure 5. Increased potency of PhScN as a systemic therapy to prevent breast cancer bone colony progression.
Figure 6. Colocalization of Ac-PhscNGGK-Bio with DiI in lung–extravasated SUM149PT cells.

Table 1. Inhibition of α5β1–mediated invasion of basement membranes by SUM149PT and MDA-MB-231 cells: IC50 and DRI values for PhScN and PHSCN derivatives.
Table 2. Invasion Inhibition: IC_{50} and K_d's for biotinylated PhScN and PHSCN derivatives.
Table 3. Extravasation Inhibition IC50's and DRI's: PhScN, PHSCN, and PhScNGGK–dendrimer, cN–MAP.
Table 4. Effects of PhScN or PHSCN pretreatment on lung colonization.
Figure 7. TIC (total ion current) chromatogram from an LC-MSMS of PHSCN and MRFA mixture.
Figure 8. CID (collision–induced dissociation) fragmentation of doubly–charged ion at 597.73 m/z. Fragment ions B4, A2, Y2,Y3, and Y4 containing S-S cross-linked peptides confirm S–S bond formation between two thiols of cysteine.

BODY:

Increased invasion inhibitory potency of Ac-PhScN-NH_2, and the Ac-PhScNGGK-MAP dendrimer.

The Hill–Slope plots for the effects of varying concentrations of Ac-PhScN-NH_2, Ac-PHSC(S–OAc)N-NH_2 or Ac-PHSC(S–Me)N-NH_2 on MDA-MB-231 breast cancer cell invasion *in vitro* are shown in Figure 1A. Similar Hill–Slope plots were obtained for SUM149PT, as summarized in Table 1. Moreover, to demonstrate that PhScN targets α5β1–mediated invasion specifically, we also utilized a peptide consisting of the α5β1 integrin–specific ligand [16] from the ninth module of the fibronectin cell–binding domain, Ac-PHSRN-NH_2 (PHSRN) to induce invasion under serum–free conditions, as shown in Figure 1B. Table 1 summarizes the half maximal invasion inhibitory concentration (IC_{50}) and the dose reduction index (DRI) values for PHSCN and its S–methylated [C(Me)N] or S–acetylated [C(O-Ac)N} cysteine derivatives for both MDA-MB-231 and SUM149PT cell lines. IC_{50} and DRI values based on pg/ml or molar (M) concentrations are also presented for Ac-PhScN-NH_2 (PhScN) and the Ac-PhScNGGK-MAP polylysine dendrimer (cN-MAP) for invasion induced by either serum or PHSRN, under serum–free conditions. As shown here, PhScN was a highly potent inhibitor of serum–free, PHSRN–induced invasion by both MDA-MB-231 and SUM149PT cells. These results demonstrate that PhScN targets α5β1–mediated invasion specifically in both cell lines.

Figure 1.

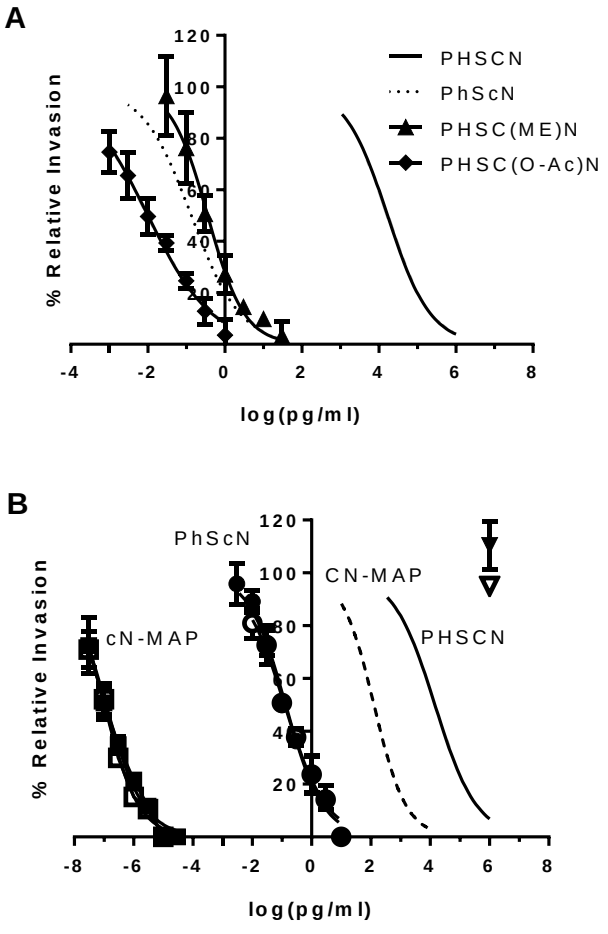

Table 1. Inhibition of α5β1–mediated invasion of basement membranes by SUM149PT and MDA-MB-231 cells: IC50 and DRI values for PhScN and PHSCN derivatives

		SUM149 PT		MDA-MB-231		DRI	
		IC_{50}		IC_{50}			
		FBS	PHSRN	FBS	PHSRN		
	Mw	pg/ml	pg/ml	pg/ml	pg/ml	pg/ml	M
PHSCN	598	8980	67120	16800	14500	1	1
CN-MAP	7500	125	152	128	90	10^2	10^3
C(Me)N	614	0.27	--	0.36	--	10^4	10^4
C(O-Ac)N	640	0.01	--	0.01	--	10^6	10^6
PhScN	598	0.076	0.081	0.135	0.124	10^5	10^5
cN-MAP	7500	4.4×10^{-8}	7.6×10^{-8}	1.3×10^{-7}	1.1×10^{-7}	10^{11}-10^{12}	10^{12}-10^{13}

During the development of PHSCN for clinical trials, it was suggested that PHSCN inhibits invasion via disulfide bonding with α5β1 integrin[1]. However, the increased potencies of the S-acetylated or S–methylated PHSCN derivatives, Ac-PHSC(S–OAc)N-NH_2 or Ac-PHSC(S-Me)N-NH_2, observed for both MDAMB231 and SUM149PT cells, and also seen in prostate cancer cell lines[17], suggests that the productive mechanism is actually noncovalent; thus, covalent bonding is an unproductive side reaction. The similarity of the invasion–inhibitory potency of the PhScN peptide to that of S–acetylated or S–methylated PHSCN further suggests that the substitutions of L–His with its stereoisomer D–His, and L–Cys with its stereoisomer D–Cys accomplish the same goal as covalent modification of the cysteine side chain, i.e. the prevention of disulfide bond formation. Hence the mechanism of inhibition for both PhScN and PHSCN is noncovalent[17].

The PhScNGGK-MAP (7500) polylysine dendrimer consisting of 8 subunits of PhScN was also tested and demonstrated an astonishing 10^7–fold increased invasion–inhibitory potency over monomeric PhScN (596 Da). This increase was significantly greater than the 1000–fold increase seen when comparing PHSCNGGK-MAP and PHSCN peptide[12,13], as shown above in Table 1. This greatly increased potency demonstrates the potential for creating a multivalent peptide mimetic.

Comparison of dissociation constants (K_d) and competition binding assays for cell surface binding using biotinylated PhScN or PHSCN peptides

The composition of the PHSCN and PhScN peptides is chemically the same; however the D–stereoisomer amino acid substitutions produce differences in the orientation of the side chains on the peptide backbone. These differences could influence the binding of the compound to its target and also help explain the 100,000–fold increase in the PhScN invasion–inhibitory potency.

A binding assay using biotin–labeled PHSCN was developed during preparation for clinical trials[1]. This assay allows for determination of the dissociation constant (K_d) of a biotin–labeled peptide to suspended cells. Biotinylated derivatives of PHSCN and PhScN were obtained and first evaluated for inhibitory potency in the SU-ECM *in vitro* invasion assay. The IC_{50}'s of the new compounds, Ac-PhScNGGK-Bio and Ac-PHSCNGGK-Bio were found to be very similar to those of the parental Ac-PhScN-NH_2 and Ac-PHSCN-NH_2 peptides for both suspended MDA-MB-231 cells (Figure 2A, Table 2) and SUM149PT cells (Table 2). Hence, the presence of the additional –GGK residues and the biotin moiety did not adversely affect the invasion–inhibitory potencies in MDA-MB-231 and SUM149PT cells.

As shown in Figure 2B and summarized in Table 2, the dissociation constant (K_d) values for thew Ac-PHSCNGGK-Bio binding to suspended SUM149PT and MDA-MB-231 cells were estimated to be 0.028 and 0.032 μM, respectively. The K_d values for Ac-PhScNGGK–Bio were estimated to be 0.029 and 0.053 μM for suspended SUM 149PT and MDA-MB-231 cells, respectively. The values are very similar for both PHSCN

and PhScN, thereby supporting the hypothesis that the improved invasion–inhibitory potency of PhScN (Table 1) is due to the elimination of the nonproductive covalent side reaction, rather than to tighter binding as a result of orienting the D–cysteine side chain to the opposite side of the peptide ligand. This is also consistent with our observations for metastatic prostate cancer cell lines[17], and demonstrates that the noncovalent interaction is the key to invasion–inhibitory efficacy.

Competition assays were also performed to confirm that PHSCN and PhScN interact with the same binding site in breast cancer cells, as was found for DU 145 and PC-3 prostate cancer cells[17]. Results of competition assays, in which suspended MDA-MB-231 cells were incubated with a constant concentration (0.1 μM) of biotinylated Ac-PHSCNGGK–Bio and varying concentrations of unlabeled Ac-PhScN-NH_2, are presented in Fig. 2C. These results show that the dissociation of Ac-PHSCNGGK–Bio with increasing concentrations of unlabeled Ac-PhScN-NH_2 occurs over approximately 2 orders of magnitude, and demonstrates that PhScN and PHSCN are competing for the same binding site on MDA-MB-231 cells[18]. Similar results were obtained for SUM149PT, *data not shown*.

Figure 2

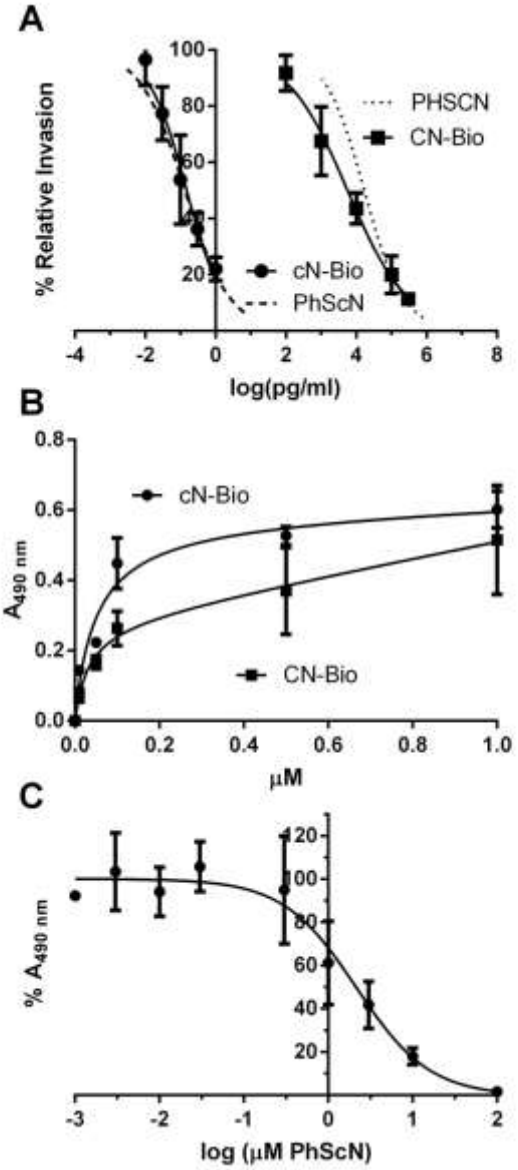

Table 2. Invasion Inhibition: IC_{50} and K_d 's for biotinylated PhScN and PHSCN derivatives

		SUM149 PT		MDA-MB-231	
	Mw	IC_{50} pg/ml	Kd μM	IC_{50} pg/ml	Kd μM
Ac-PHSCN-NH_2	598	8980	NA	16800	NA
Ac-PhScN-NH_2	598	0.076	NA	0.124	NA
Ac-PHSCNGGK–Bio	1100	8637	0.028 ± 0.02	5622	0.032 ± 0.03
Ac-PhScNGGK–Bio	1100	0.051	0.029 ± 0.02	0.15	0.053 ± 0.03

Increased potencies of the PhScN peptide and PhScNGGK–MAP dendrimer as inhibitors of lung extravasation

Extravasation of tumor cells to the lung and successful colonization are late stages in breast cancer progression that are ultimately fatal. Hence, prevention of extravasation which leads to colony formation would increase life expectancy. Cell surface α5β1 integrin has been shown to play a key role in extravasation[17]. Furthermore, PHSCN has been shown to inhibit α5β1–mediated invasion specifically [1,4,,12,13,19–22], and to reduce or prevent lung metastasis in preclinical models[1,4,,12,13,17, 19–22] . Moreover, systemic PHSCN(ATN-161) was found to be well–tolerated, and to delay disease progression for 4 to 14 months in Phase I clinical trial[23]. Since Ac-PhScN-NH_2 exhibited a 100,000–fold greater inhibitory potency *in vitro,* on naturally occurring basement membranes[17], we compared the efficacies of PhScN and PhScNGGK–MAP with the PHSCN peptide as inhibitors of lung extravasation by breast cancer cells in athymic mice.

To assess their efficacies, treatment groups–each consisting of 10 mice–received a single systemic pretreatment with the appropriate peptide or dendrimer concentrations by tail vein injection. Then, DiI–labeled MDA-MB-231 or SUM149PT cells, briefly prebound to the appropriate concentrations of peptide, were injected into the tail veins of the pretreated mice. The lungs were extracted 24 hours later. A graph of the mean number of extravasated cells per section, and the resulting dose response curves for inhibition of SUM149PT and MDA-MB-231 lung extravasation are presented in Figures 3A and 3B, respectively; and the IC_{50} and DRI values are summarized in Table 3. Each point shows the mean and SEM obtained from confocal microscopy analysis of 20 sections of 10 micron thickness, each separated by 200 microns, from each of a total of 10 mice for each treatment group. Figure 3C shows typical examples of sectioned lung tissue for MDA-MB-231 extravasation analyzed by confocal microscopy after pretreatment with 100 ng/ml Ac-PhScN-NH_2 or 100 ng/ml Ac-PHSCN-NH_2, compared to untreated control. Figure 3D shows typical examples of sectioned lung tissue for SUM149PT extravasation analyzed by confocal microscopy after pretreatment with 100 ng/ml Ac-PhScN-NH_2 or 100 ng/ml Ac-PHSCN-NH_2, compared to untreated control. Images represent the merged composite of fluorescent DiI–labeled cells shown in orange; fluorescent blue–stained nuclei from DAPI–containing mounting medium; and fluorescent green anti–actin staining of cytoplasm. Lung extravasated MDA-MB-231 and SUM149PT cells had very similar appearance, as shown in Figs. 3C and 3D. The median–affect plots of Fig. 3B show that increasing concentrations of the PhScN or PHSCN peptides, or the PhScNGGK–MAP dendrimer, decrease SUM149PT and MDA-MB-231 extravasation in a log–linear fashion, with similar relative potencies in both cell lines. In contrast, pretreatment with 1 □g per ml Ac-hSPNc-NH_2 scrambled sequence control, followed by a single systemic treatment at the equivalent dose, had no inhibitory effect on lung extravasation, *data not shown*. As shown In Table 3, the PhScN peptide appears to be 100– to 1000–fold more potent than the PHSCN peptide at inhibiting lung extravasation by both SUM149PT and MDA-AB-231 cells. Moreover, the

PhScNGGK–MAP dendrimer appears to be 100,000– to 1,000,000–fold more potent than PHSCN at inhibiting lung extravasation by SUM149PT and MDA-MB-231 (Table 3). These *in vivo* values correlate well with those seen in the *in vitro* invasion assay (Table 1) using isolated, naturally occurring basement membranes.

Figure 3.

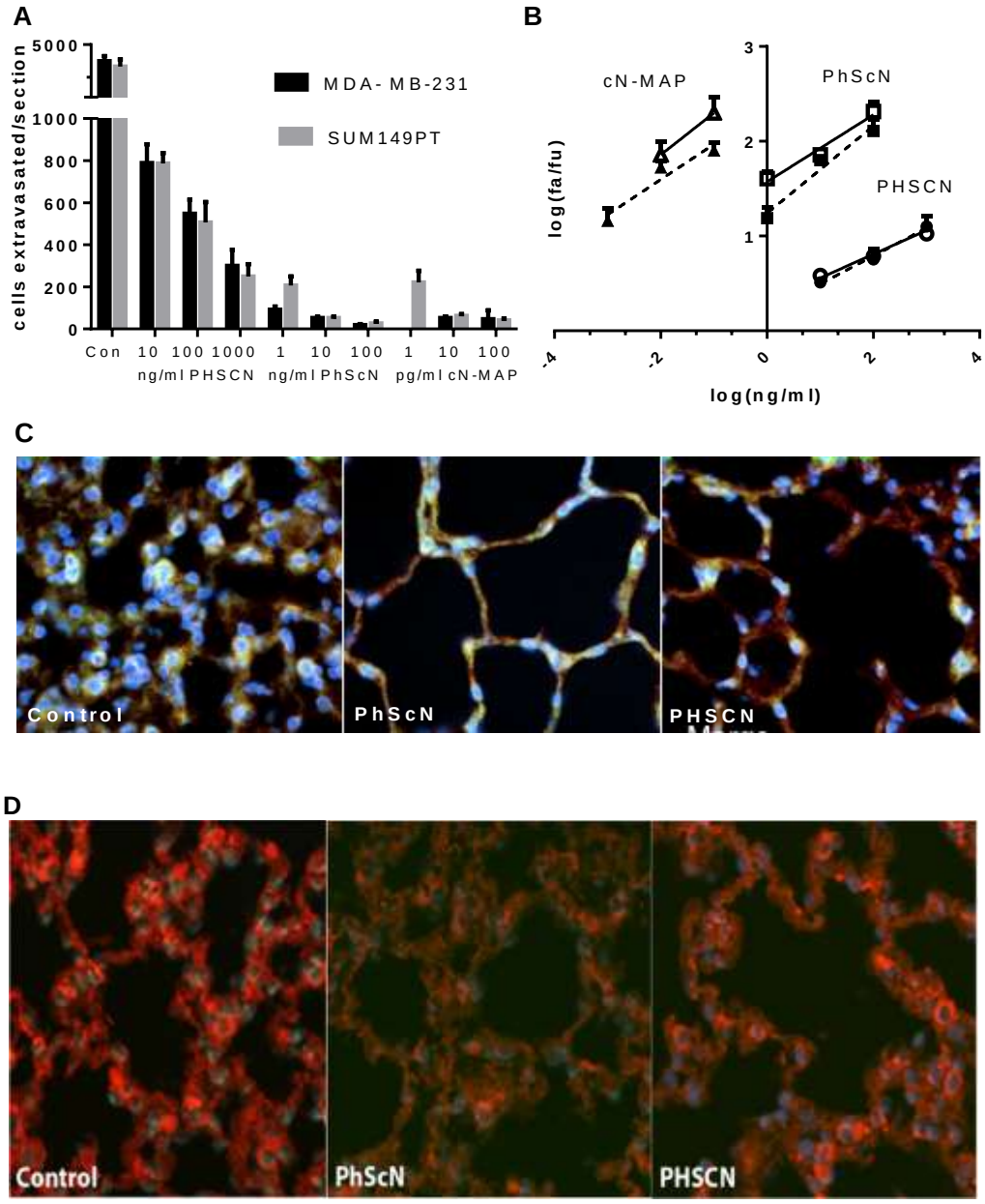

Table 3. Extravasation Inhibition: IC50's and DRI values for PhScN, PHSCN, and PhScNGGK-MAP.

		SUM149PT	MDA-MB-231	DRI	
		IC_{50}	IC_{50}		
	Mw	pg/ml	pg/ml	pg/ml	M
PHSCN	598	214	61	1	1
PhScN	598	2.0	0.036	10^2-10^3	10^2-10^3
cN-MAP	7500	0.0005	0.0006	10^5	10^6

Increased potency of the PhScN peptide as an inhibitor of lung colonization

Since extravasated cancer cells may be limited in their ability to establish a metastatic colony[24], effects of PhScN or PHSCN pretreatment on subsequent lung colony formation were also evaluated after extravasated cells were allowed to grow *in vivo* without further treatment for 6 weeks. Figure 4A presents a comparison of the efficacies of prebinding various concentrations of PhScN or PHSCN to suspended, DiI–labeled SUM149PT or MDA-MB-231 cells on lung colonization after tail vein injection. The dose response curves are presented as median effect plots in Fig 4B, and the IC_{50} and DRI values are summarized in Table 4. Each value represents the mean and SEM from a total of 20 sections of 10 micron thickness, each separated by 200 microns, from each of 10 mice per treatment group. Figure 4C shows typical examples of DiI–labeled MDA-MB-231 lung colonies in fluorescent actin– and DAPI–stained lung tissue after no treatment, and after prebinding of the injected cells to 100 ng/ml of either PHSCN or PhScN. DiI–labeled SUM149PT lung colonies had a similar appearance, *data not shown*. Since induction of cell death, for example by apoptosis, could contribute significantly to the potency of systemic PhScN as an inhibitor of lung colonization, we assessed apoptosis induction *in vitro* in adherent SUM149PT cells by examining the effects of a 1–hour treatment with a range of Ac-PhScN-NH_2 concentrations. Figure 4D presents a typical Western blot indicating that PhScN does rapidly induce a dose–dependent upregulation of activated Caspase–3 in adherent SUM149PT cells; but concentrations required are 1,000– to 100,000–fold higher than those required for lung colonization inhibition. Effects of 500 □g Ac-hSPNc-NH_2 per 10^6 SUM149PT cells, are also shown. The lack of activated Caspase–3 upregulation in SUM149PT cells treated with hSPNc demonstrates that although high PhScN concentrations are required for the upregulation of activated Caspase–3, the effect is sequence–specific.

Qualitatively, MDA-MB-231 and SUM149PT respond similarly to both PHSCN and PhScN; however, the corresponding IC_{50} values are 10– to 100–fold higher for SUM149PT cells (Table 3). This may be due to the nature of the specific cell preparations or perhaps the differences between a metastatic cancer line (MDA-MB-231) and an inflammatory cell line (SUM149PT). Regardless of the IC_{50} values, the overall DRI values determined for both MDA-MB-231 and SUM149PT cells suggest that PhScN is 1000– to 10,000–fold more potent at preventing lung colonization than PHSCN. Since stress, due to hypoxia for example, has been shown to increase activated $\alpha5\beta1$ receptor levels[25], we checked whether Ac-PhScN-NH_2 treatment could induce apoptosis in breast cancer cells. We found that very elevated concentrations of (100, 200 and 300 μg/ml) of Ac-PhScN-NH_2 could induce caspase-3 upregulation in adherent SUM149PT cells; but that lower levels (10 and 50 μg/ml) had no effect, as shown in Figure 4D.

Figure 4.

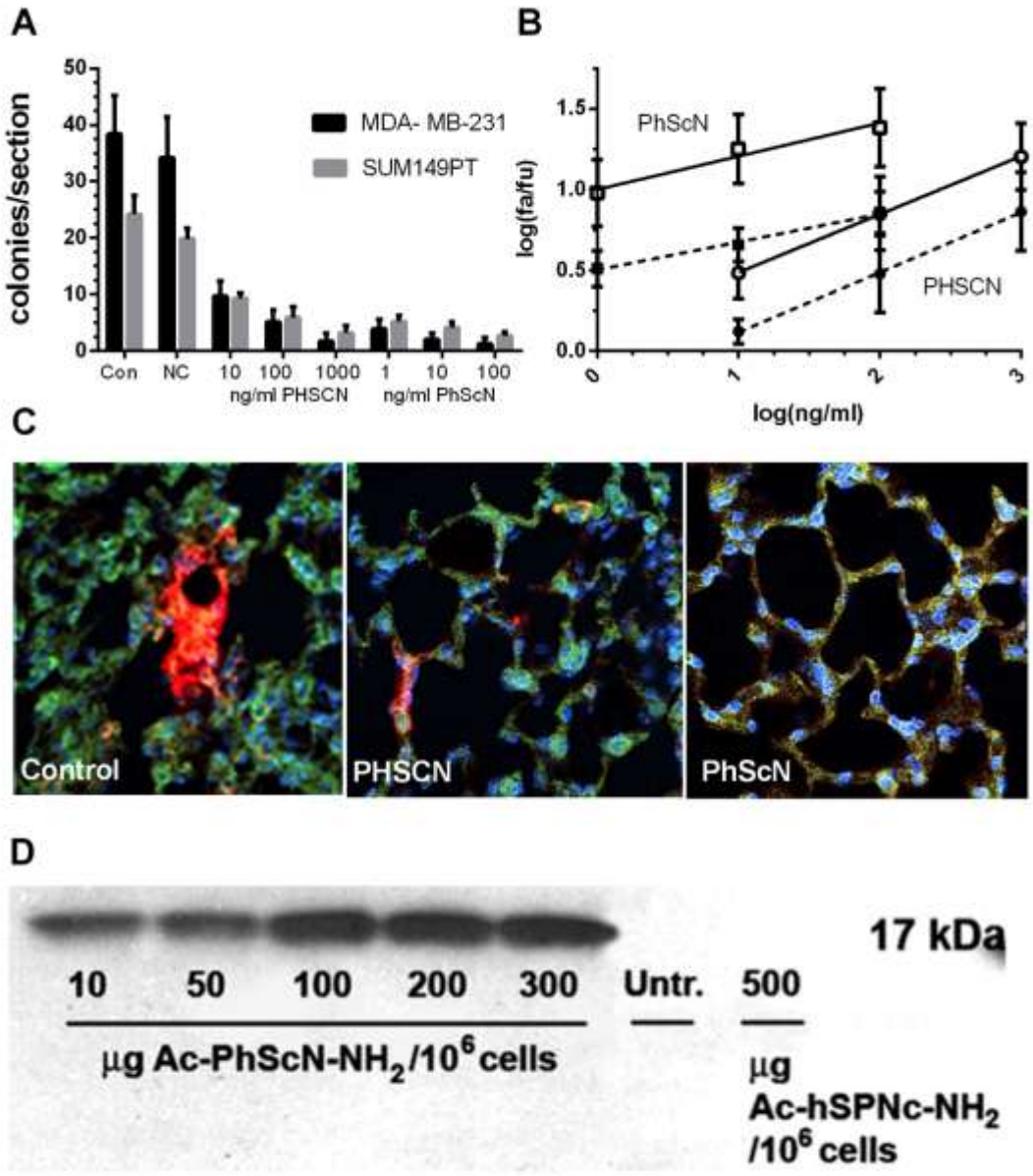

Table 4 Effects of PHSCN or PhScN pretreatment on lung colonization.

	SUM149PT	MDA-MB-231	DRI	
	IC50	IC50		
	pg/ml	pg/ml	pg/ml	M
PHSCN	4890	450	1	1
PhScN	1.27	0.014	10^3-10^4	10^3-10^4

Inhibition of bone metastasis progression by systemic PhScN therapy of mice after intratibial injection of metastatic human MDA-MB-231 breast cancer cells

In breast cancer, metastasis to the bone is usually an earlier disease event than lung colonization[26]. The interaction of bone–metastatic breast cancer cells with the surrounding bone marrow and matrix is best described by the "vicious cycle" model[27]. In this model, parathyroid hormone related protein (PTHrP) expressed by breast cancer cells after bone colonization[28], stimulates progression and enhances osteoclastic bone resorption through its effects on osteoblasts[29,30]; moreover, it has been shown to enhance osteoclastic bone resorption in MDA-MB-231 bone metastases[31]. Furthermore, PTHrP is a key mediator of osteoclast activation[25]. In response to signals from metastatic breast cancer cells, bone lining osteoblasts express osteoclast–stimulatory factors, like receptor activator of nuclear kappa B ligand (RANKL)[32], which stimulate osteoclast precursors to generate multinucleated osteoclasts[33]. These activated osteoclasts resorb mineralized bone matrix[34,35] to release sequestered growth factors that promote metastatic growth by stimulating angiogenesis[36-38]. Activated $\alpha5\beta1$ receptors of microvascular endothelial cells interact with the PHSRN sequence of pFn cell–binding domain fragments to induce angiogenic invasion[5]. Furthermore, MDA-MB-231 colonies in the bones of athymic mice have been shown to induce angiogenesis in osteolytic metastases[39]. The identification of $\alpha5\beta1$ integrin as the primary integrin fibronectin receptor on human bone marrow stroma[40] suggests that PhScN could be effective in reducing bone metastases.

Microvascular endothelial cells (hmvec) were tested in our *in vitro* invasion assay as described[5], and both PHSCN and PhScN were confirmed to block invasion. The IC_{50} values were similar to those determined for MDA-MB-231 and SUM149PT cells; and PhScN demonstrated a 6.3×10^{4}–fold increase in potency over PHSCN (PhScN IC_{50}, 1.3×10^{-13} M; PHSCN IC_{50}, 8.4×10^{-9} M).

To assess the effects of PHSCN and PhScN on established bone metastases, DiI–labeled MDA-MB-231 cells were injected intratibially into athymic mice, and were allowed to grow into intra-osteal colonies for two weeks before thrice-weekly systemic treatments of 5 or 50 mg/kg of PhScN or PHSCN, respectively, were initiated. ***The MDA-MB-231 cells were not pretreated with either PhScN or PHSCN peptide prior to intratibial injection*. Furthermore, mice received no systemic treatments of any kind for 2 weeks after intratibial injection.** After 2 weeks of untreated intratibial MDA-MB-231 growth, systemic treatments were initiated. Treatments were continued for 24 days; with each mouse receiving a total of 10 systemic treatments. As shown in Fig. 5A, 50 mg/kg systemic PhScN monotherapy reduced bone colony progression by about 77%, compared to a reduction of 57% for 5 mg/kg PHSCN. Results of median effect analysis, shown in Fig. 5B, indicate a dosage IC_{50} of 0.4 mg/kg for PhScN and 10 mg/kg for PHSCN. **The calculated DRI value indicates that PhScN is 25–fold more potent than PHSCN as a systemic inhibitor of bone metastasis progression.** As seen in the examples obtained from confocal microscopy, shown in Fig. 5C, few MDA-MB-231 cells remained in the intratibial bone marrow of mice treated with 50 mg/kg PhScN; whereas significantly more cells were present in the marrow of mice treated with 50 mg/kg PHSCN. As shown in the image from mice receiving 50 mg/kg PHSCN therapy, bone colonies appeared to be either extravascular, or closely associated with the vasculature.

Figure 5.

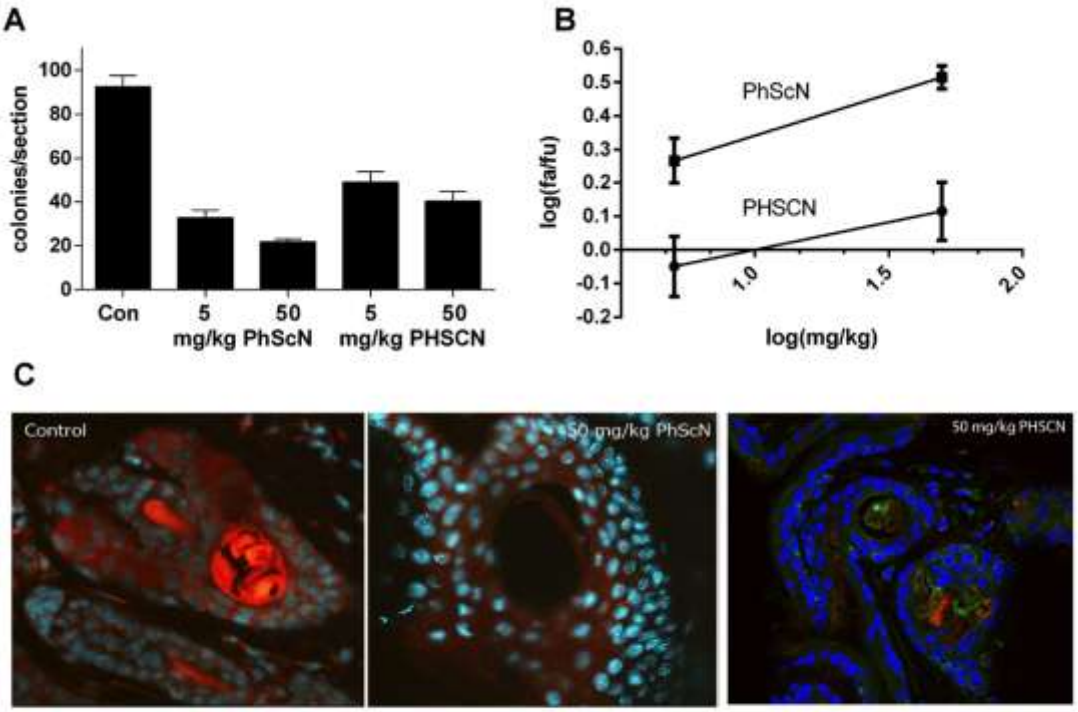

Colocalization of Ac-PhScNGGK-Bio with DiI in extravasated breast cancer cells

Since additional nodal metastases are identified in at least 20% of patients who undergo a completion axillary lymph node dissection (ALND) following a sentinel lymph node biopsy (SLNB) in which micrometastases were identified, the use of SLNB alone for staging the axilla may lead to the underestimation of the extent of nodal disease in 20% of cases[41]. Hence, a more efficient means of detecting bone–metastatic disease would be very beneficial. The potency of Ac-PhScN-NH_2 as a noncovalent inhibitor of $\alpha5\beta1$–mediated invasion *in vitro*, as well as lung extravasation and metastasis, and bone colonization, suggested that the labeled PhScN peptide, Ac-PhScNGGK-Bio, might be an effective detection agent for extravasated, potentially metastatic breast cancer cells in sectioned biopsies. Thus, we assessed the ability of Ac-PhScNGGK-Bio to colocalize with DiI in lung–extravasated SUM149PT inflammatory breast cancer cells after they were introduced by tail vein injection. As shown in Figure 6A, 5.0 to 50.0 □g per ml of biotinylated Ac-PhScNGGK-Bio peptide labeled 89% to 90% of extravasated SUM149PT cells in lung tissue sections of athymic mice, harvested 24 h after intravenous injection. Figure 6B shows representative images of detection of DiI–labeled SUM149PT, with and without colocalization of Ac-PhScNGGK–Bio. These results suggest that labeled PhScN could be an efficient agent for detecting extravasated breast cancer cells, which specifically express activated $\alpha5\beta1$ integrin and hence are invasive and potentially metastatic.

Figure 6.

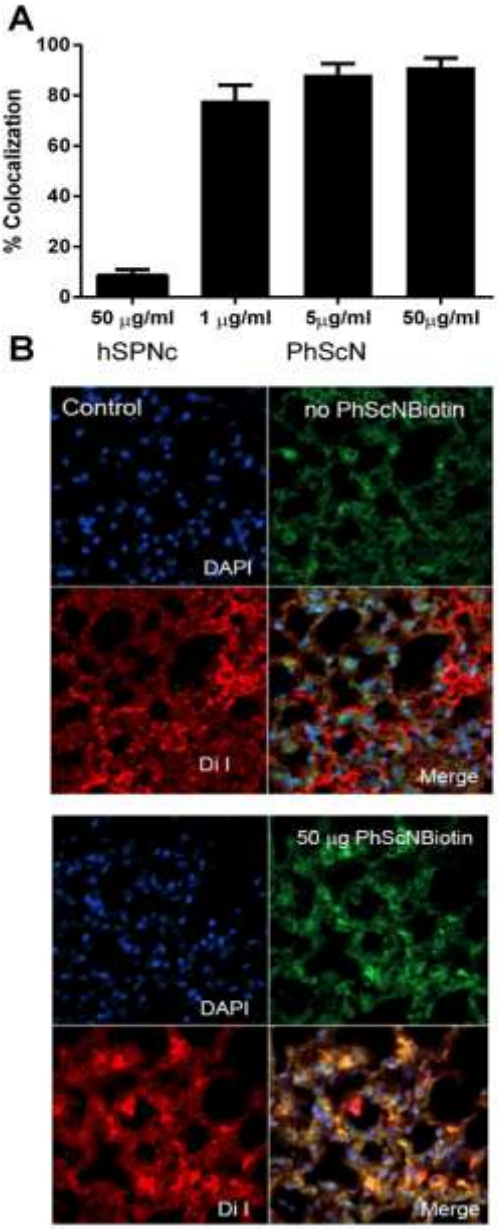

Since recurrent or metastatic disease develops in at least 40% of early breast cancer patients[42], with bone metastasis occurring in most[27], there is an urgent need for an effective, well–tolerated, therapy which can prevent both metastatic and angiogenic invasion. As summarized below in **Scheme 1**, the ability to inhibit activated α5β1 integrin receptors on metastatic breast cancer cells and their associated angiogenic, microvascular endothelial cells, may form the basis of an effective targeted therapy to inhibit the vicious cycle of breast cancer bone metastasis progression.

Overexpression of parathyroid hormone related protein, PTHrP, in MDA-MB-231 breast cancer cells has been shown to induce a 10– to 25–fold upregulation of α5 integrin promoter activity resulting in increased α5β1 integrin levels[43]. Furthermore, radiation has also been shown to stimulate invasion by inducing surface

upregulation of activated α5β1 integrin[44]. Because α5β1 integrin mediates metastatic invasion[4, 10, 12,13, 45] to cause systemic dissemination[3,4 ,10], as well as microvascular endothelial cell invasion[5] to promote angiogenesis, we have pursued α5β1 as a therapeutic target[3-5,10-13,17]. Matrix metalloproteinase–1 (MMP1), is induced by the interaction of α5β1 integrin with the PHSRN sequence of the fibronectin cell binding domain[45], and mediates both angiogenic and metastatic invasion by breast, prostate, and pancreatic cancer cells[3,4,5,10,,44,]. MMP-1 has also been shown to activate the protease activated receptor–1 (PAR-1) gene in both breast cancer[46] and endothelial cells[47], thereby promoting breast cancer invasion, as well as angiogenesis. PTHrP has been shown to stimulate osteoblasts to induce osteoclast progenitor differentiation into active osteoclasts, which mediate bone resorption, thereby releasing epidermal growth factor (EGF)–like growth factors to further stimulate bone metastasis progression[48]. Our research has shown that overexpression of receptor tyrosine–protein kinase erbB-2 or HER2, a member of the EGF receptor family, causes constitutive, serum–induced, pFn–dependent α5β1–mediated invasion by immortalized mammary epithelial cells[49], due to surface down regulation of the invasion–inhibitory α4β1 fibronectin receptor[50]. The results of these studies thus suggest that inflammatory growth factors released as a result of bone resorption induce upregulation of activated α5β1 receptors to promote metastatic invasion of the bone, as well as angiogenic invasion to support bone colony progression. Hence, as summarized in Scheme 1, the α5β1 integrin fibronectin receptors of both bone–metastatic breast cancer cells and the microvascular endothelial cells of the bone marrow play a key role in the vicious cycle of bone metastasis.

Scheme 1.

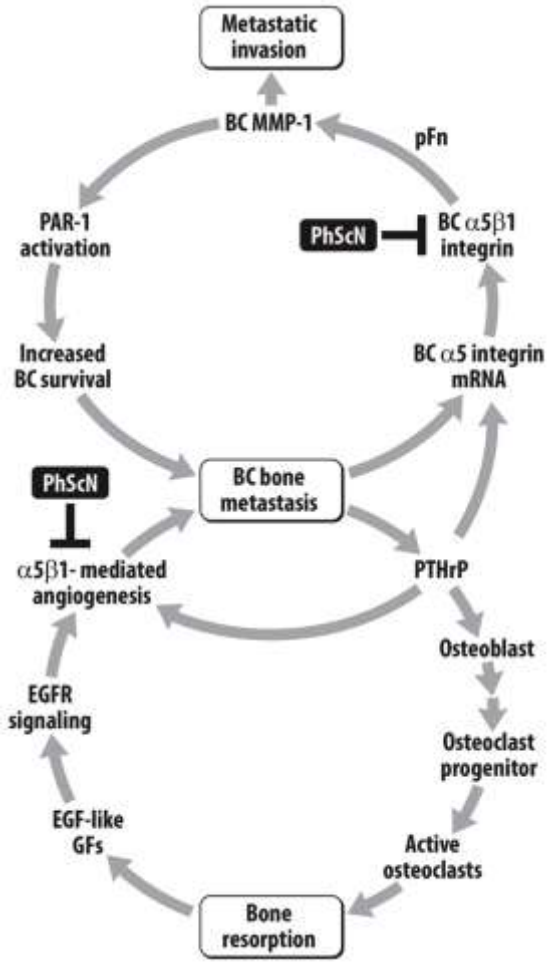

Figure Legends

Figure 1. Hill–Slope plots of increased invasion inhibitory potency of Ac-PhScN-NH_2 peptide, Ac-PhScNGGK-MAP dendrimer, and the cysteine–modified, methylated (Me) or acetylated (O-Ac) peptides, Ac-PHSC(Me)N-NH_2 and Ac-PHSC(O-Ac)N-NH_2 for MDA MB-231 cells. Panel A, effects on FBS–induced invasion by cysteine–modified Ac-PHSC(Me)N-NH_2 or Ac-PHSC(O-Ac)N-NH_2, and D–His, D–Cys containing Ac-PhScN-NH_2 peptides. Symbols are denoted in the figure. X axis, log peptide concentration in pg per ml; Y axis, mean relative percentages of invaded cells (+/- SD). IC_{50} and DRI values are summarized in Table 1. Panel B, Increased potencies of PhScN peptide and PhScN dendrimer for both serum–induced, and serum–free, Ac-PHSRN-NH_2 (1 □g/ml) –induced, α5β1–mediated invasion. Circles denote Ac-PhScN-NH_2, and squares denote Ac-PhScNGGK-MAP dendrimer, closed symbols denote FBS induced and open symbols denote Ac-PHSRN-NH_2 (1 □g/ml) induced. X-axis, log peptide concentration in pg/ml; Y-axis, mean relative percentage of invaded cells (±SD). The solid and dashed line represent published values for Ac-PHSCN-NH_2 and Ac-PHSCNGGK-MAP respectively.

Figure 2. Panel A, Hill–Slope plots of invasion inhibition by biotinylated derivatives of PHSCN and PhScN for MDA-MB-231 cells induced by FBS. Specific agents (CN-Bio, Ac-PHSCNGGK-Bio; cN-Bio, Ac-PhScNGGK-Bio) are listed on the right. X axis, log peptide concentration in pg per ml; Y axis, mean relative percentages of invaded cells (+/- SD). IC_{50} and DRI values are summarized in Table 2. Panel B, K_d binding assays for Ac-PHSCNGGK-Bio (CN-Bio) and Ac-PhScNGGK-Bio (cN-Bio) peptides with suspended MDA MB231 cells. Plots were fit using a total binding equation to account for nonspecific binding(Motulsky and Neubig 2010). Panel C, Competition binding was determined by incubating suspended MDA-MB-231cells with a constant concentration of 0.1 □M Ac-PHSCNGGK–Bio (labeled) and varying amounts of unlabeled Ac-PhScN-NH_2. Plot was fit using a competitive inhibition equation[18].

Figure 3. Increased extravasation inhibition by Ac-PhScN-NH_2 or Ac-PhScNGGK–MAP prebinding, relative to Ac-PHSCN-NH_2 peptide. Panel A, Y axes, average cells extravasated/section; X Axes, Con, control; 10, 100, 1000 ng/ml PHSCN; 1, 10, 100 ng/ml PhScN; 1, 10, 100 pg/ml PhScNGGK-MAP. Panel B, Median–affect plot for extravasation into lung after prebinding with PHSCN (circles), PhScN (squares) or PhScN-MAP (triangles); open symbols, MDA-MB231 cells; closed symbols, SUM 149 PT cells. X axes, log peptide concentration in ng/ml; Y axes, mean log fraction affected/fraction unaffected (f_a/f_u) +/- SEM. IC_{50} and DRI values are summarized in Table 3. Panel C**.** Typical examples of sectioned lung tissue for MDA-MB231 extravasation analyzed by confocal microscopy after pretreatment with 100 ng/ml Ac-PhScN-NH_2 or 100 ng/ml Ac-PHSCN-NH_2, compared to untreated control. Panel D. Typical examples of sectioned lung tissue for SUM149PT extravasation analyzed by confocal microscopy after pretreatment with 100 ng/ml Ac-PhScN-NH_2 or 1000 ng/ml Ac-PHSCN-NH_2, compared to untreated control. Images represent the merged composite of DiI-labeled cells shown in orange; blue stained nuclei from DAPI Mounting Medium; green tissue from actin staining.

Figure 4. Increased inhibition of lung colonization by Ac-PhScN-NH_2 prebinding, relative to Ac-PHSCN-NH_2. Panel A, Y axes, average colonies/section; X Axes, Con, control; NC, 100 ng/ml HSPNC; 10, 100, 1000 ng/ml PHSCN; 1, 10, 100 ng/ml PhScN Panel B, Median–effect plot for lung colony formation after prebinding to PHSCN (circles) or PhScN (squares). Closed symbols, dotted lines, SUM149PT cells; Open symbols, solid line MDA-MB-231 cells. X axes, log peptide concentration in ng/ml. Y axes, mean log fraction affected/fraction unaffected (f_a/f_u) +/- SEM. IC_{50} and DRI values are summarized in Table 4. Panel C. Typical examples of

sectioned lung tissue for MDA-MB231 colonization analyzed by confocal microscopy after pretreatment with 100 ng/ml Ac-PhScN-NH_2 or 100 ng/ml Ac-PHSCN-NH_2 compared to untreated control. Images represent the merged composite of DiI-labeled cells shown in orange; blue stained nuclei from DAPI Mounting Medium; green tissue from actin staining. Panel D. Example of a Western blot showing dose–dependent upregulation of activated Caspase–3 in adherent SUM149PT cells by a one–hour treatment with a range of Ac-PhScN-NH_2 concentrations (10, 50, 100, 200, or 300 □g/10^6 cells). Micrograms of Ac-PhScN-NH_2 per million SUM149PT cells are indicated. Effects of an elevated concentration of a scrambled sequence control, 500 □g Ac-hSPNc-NH_2 per 10^6 SUM149PT cells, are also shown.

Figure 5. Increased potency of PhScN as a systemic therapy to prevent breast cancer bone colony progression in athymic mice. A. Anti–metastatic potencies of systemic PhScN (Ac-PhScN-NH_2) vs. PHSCN (Ac-PHSCN-NH_2) for reducing MDA-MB-231 bone marrow progression in athymic mice. Y axes, average cells per section; X Axes, Con, untreated control; 5 and 50 mg/kg PhScN; 5 and 50 mg/kg PHSCN. B. Median effect plot for effects of PhScN vs PHSCN on bone marrow progression, *X* axis, log peptide dosage level (mg/kg); *Y* axis, mean log fraction affected/fraction unaffected (fa/fu) +/- SEM. C. Examples of bone marrow from untreated mice, and from mice treated with a total of 10 thrice–weekly tail vein injections: 50 mg/kg PhScN or PHSCN. Images represent merged composites of DiI-labeled cells (orange); blue–stained nuclei (DAPI Mounting Medium); green cytoplasm (actin staining). Thus, DiI–labeled cells appear orange (Control) or green with orange inclusions (50 mg/kg PHSCN). No DiI–labeled cells appear in the image of bone marrow from 50 mg/kg PhScN–treated mice.

Figure. 6. Colocalization of Ac-PhScNGGK-Bio with DiI in lung–extravasated SUM149PT cells. A. Percentage of DiI–labeled cells in lung tissue binding to different concentrations of Ac-PhScNGGK-Bio: 1, 5, or 50 μg per ml. X axis, binding agents: hSPNc, Ac-hSPNc-NH_2 (scrambled sequence control peptide); PhScN, Ac-PhScNGGK-Bio. Y axis, mean percentage of biotinylated, DiI–labeled SUM149PT cells (+/- SEM). B. Examples of fluorescently stained lung tissue: control, no PhScNGGK-Bio; 50 μg PhScNGGK-Bio, 50 μg per ml Ac-PhScNGGK-Bio. DiI–labeled cells shown in orange; blue stained nuclei from DAPI Mounting Medium; green tissue from actin staining.

Specific Aim 3

Develop a mass spectrometry–based quantitative assay for PHSCN analogs, including PhScN, and evaluate their stabilities in human and mouse plasma.

Experimental design for quantitative assay of PHSCN analogs

An experimental approach based on mass spectrometric analysis to evaluate the stabilities of PHSCN analogs in human and mouse plasma has been designed as outlined below in Scheme 1. A known amount of target peptide is mixed with plasma and incubated at 37 °C for up to 24 hours. At specific incubation time points an aliquot is transferred to a small tube and protease reactions were quenched by adding three volumes of 50% acetonitrile with 0.5%TFA. Precipitated plasma proteins were removed by centrifugations, and a known amount of an internal standard was spiked into the supernatant containing the peptides, in order to

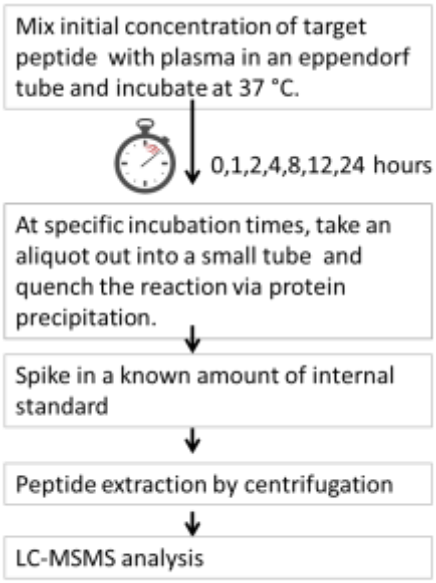

Scheme 1. Experimental workflow

increase the accuracy of quantitative measurements of LC-MS by reducing variances associated with sample preparations. MRFA (Met-Arg-Phe-Ala, monoisotopic molecular mass = 523.247.), a stable synthetic peptide with similar molecular mass to the target peptide, Ac-PHSCN-amide (monoisotopic molecular mass = 597.2328), is added into samples prior to LC-MS analysis. Stabilities of target peptides in plasma were evaluated by LC-MS.

Mass spectrometry

The LTQ-Orbitrap XL(Thermo Finnegan) connected to a 2D nanoLC(Exigent) and an autosampler in Andrews laboratory provides high mass resolution and accuracy for analytes separated on a capillary column at a flow rate of 200 nL/min, which assures confident identification of target molecules. Extracted peptides from plasma are reconstituted in 0.1% TFA and loaded into a C18 trap by autosampler and washed for 6 min at 5 microL/min with 0.1% TFA in water delivered by the LC loading pumps. Trapped peptides were introduced by switching valve into a capillary column (75 micro-m x 15 cm) custom-packed with C18 resin (3 micron) and separated over 60 min gradient at a flow rate of 200 nL/min. Analytes were introduced into the LTQ-Orbitrap via an electrospray device (Triversa Nanomate, Advion). MS and MSMS data were acquired in data-dependent mode for ions within 400-800 m/z. Figure 7 shows the total ion chromatogram (TIC) of LC-MSMS analysis of PHSCN and the internal standard MRFA.

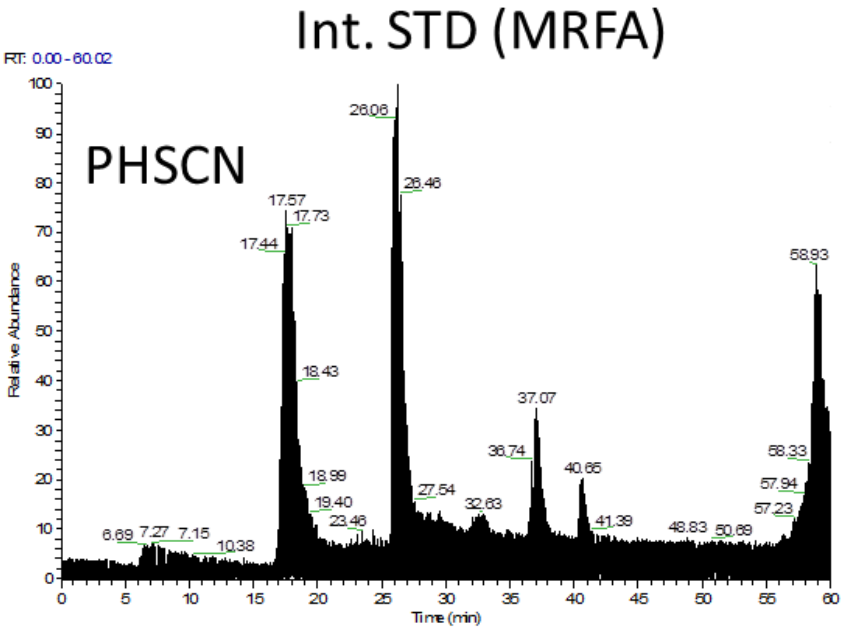

Figure 7. TIC from an LC-MSMS of PHSCN and MRFA mixture.

Quantitative assay of target peptides

Peptide quantification can be achieved by ion intensities in MS or by MSMS spectral counts in data-dependent acquisition mode. These two approaches are well established label-free quantification methods for peptides and proteins by LC-MSMS, which can be readily applied to a bioanalytical assay of therapeutic peptides. We are currently testing a new assay method, an MRM-like analysis via data-independent acquisition mode in the LTQ-Orbirap, in which ion packets within a mass range of 5 or 10 Da accumulated for a set time are co-fragmented.

One or multiple fragment ions specific to the target peptide can be monitored in MSMS based on highly accurate precursor ion mass and LC retention time. This MRM-like approach can provide a highly selective and sensitive bioanalytical assay under conditions of high chromatographic interference.

Study of collision–induced dissociation (CID) fragmentation of Ac-PHSCN-NH_s in online LC-LTQ-Orbitrap

Ac-PHSCN-NH_2 introduced into the mass spectrometer via a nanoESI device (Triversa Nanomate) was predominantly observed as singly protonated form at 598.2328 m/z. However, in online LC-MS, the peptide was observed in doubly charged dimeric forms at 597.23 m/z and 589.23 m/z. The peptide dimer ions were characterized by CID that revealed disulfide-bond formation between two peptides that was catalyzed on C18 LC, as shown in a CID spectrum of 597.23 m/z. This is a potential source of interference with the assay that can be easily addressed by incorporating reduction and alkylation of the Cys residues into the protocol prior to LCMSMS although introduction of an additional step in the process could increase the variance slightly. The reason that dimerization occurs during the LC separation but not during other manipulations or assay approaches is not clear.

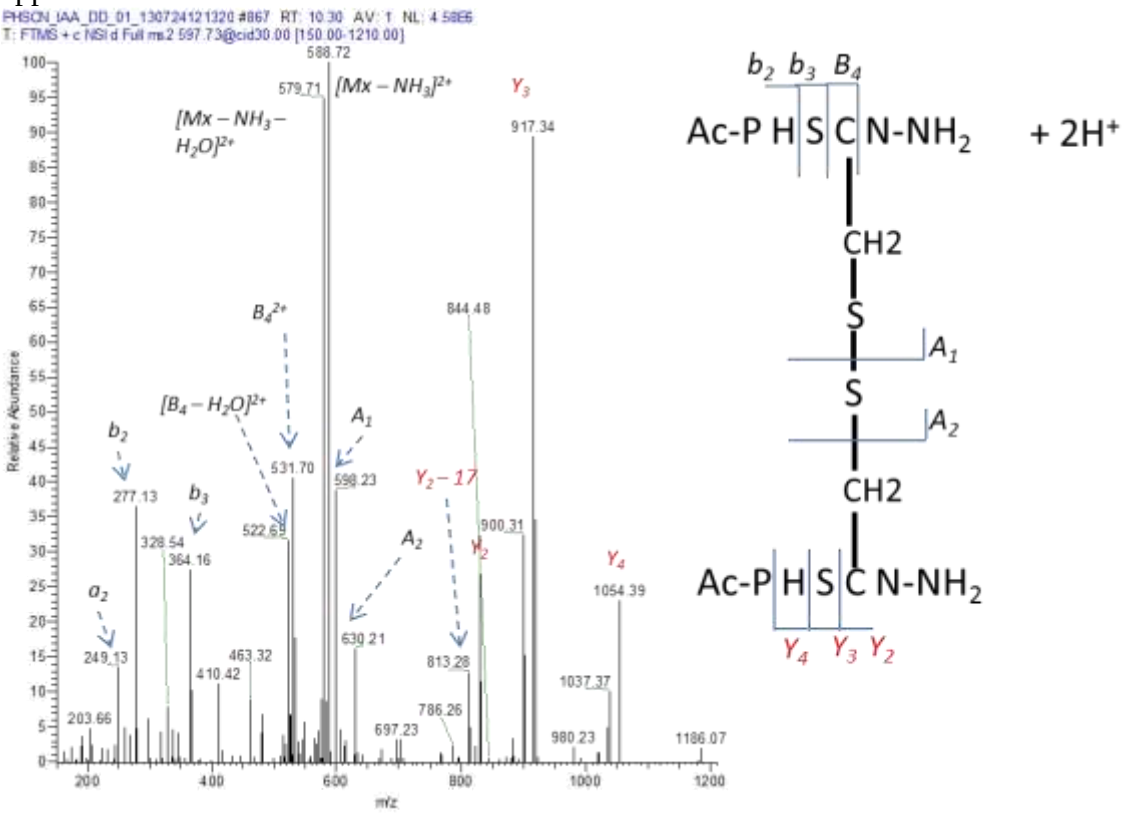

Figure 8. CID fragmentation of doubly–charged ion at 597.73 m/z (the second isotope to 597.23 m/z). Fragment ions B4, A2, Y2,Y3, and Y4 containing S-S cross-linked peptides confirm disulfide bond formation between two thiols of cysteine.

KEY RESEARCH ACCOMPLISHMENTS:

1. Determination of invasion–inhibitory potencies for a total of 12 PHSCN and PhScN derivatives, targeting α5β1 integrin–mediated invasion of naturally serum–free basement membranes by 2 metastatic human breast cancer cell lines, SUM149PT and MDA-MB-231. Demonstration that covalent S–modification by several different moieties increases invasion–inhibitory potency by 100,000– to 1,000,000–fold, and that a 1,000,000–fold increase in potency is also obtained by substiution of D–His and D–Cys. These results

demonstrate that the reason for the greatly increased invasion–inhibitory potency of PhScN is the suppression of covalent disulfide bond formation between the PHSCN sequence and its integrin target, and hence they are a key step in the determination of the PhScN target site on α5β1 integrin receptors of breast cancer cells.

2. Determination of invasion–inhibitory potencies of PHSCN and PhScN peptides, containing BPM–derivatized cysteine or D–cysteine. The greatly increased invasion–inhibitory potencies of the BPM–modified PHSCN and PhScN peptides also confirm the noncovalent nature of invasion inhibition by the PhScN peptide.

   Research accomplishments 1 and 2 complete Specific Aim 1 of the SOW.
3. Crosslinking with BPM–derivatized peptides, after integrin α5β1 activation with divalent cations, and analysis by Western blotting. Successful crosslinking with biotin labeled peptides, modified either at the cysteine or on the C–terminus, is anticipated to pave the way for protein enrichment and binding site identification by MS/MS. Our experiments demonstrating specific tagging of the integrin target indicate that significant scale-up will be required to obtain sufficient quantities for identification of the binding domains.
4. Determination of binding constants for PHSCNGGK-Bio and PhScNGGK-Bio on MDA-MB-231 and SUM149PT cells, and demonstration of their similarity provides the basis for acquiring information on any steric hindrances introduced by modification of the ligands not detected in functional invasion assays.
5. Demonstration that PHSCNGGK-Bio and PhScNGGK-Bio compete for the same binding site on SUM149PT and MDA-MB-231 cells. The results of these binding assays, in conjunction with the functional invasion inhibition results shown in Table 1, will allow a more complete profile of the peptide ligand properties and their functional effects on α5β1 integrin–mediated invasion. Moreover, these results provide key support of the hypothesis that the increased potency of the PhScN peptide results from suppression of covalent, disulfide bond formation with the integrin target.

   Research accomplishments 3, 4, and 5 provide key support towards accomplishing Specific Aim 3 of the SOW.
6. Demonstration of CID fragmentation of Ac-PHSCN-NH_2 in online LC-LTQ-Orbitrap indicates that development of a mass spectrometry–based quantitative assay for PHSCN analogs, including PhScN, for the purpose of evaluating their stabilities in human and mouse plasma (Specific Aim 3) is feasible although the methods to suppress the formation of disulfide dimers during the separation procedure must be developed.

REPORTABLE OUTCOMES: The following manuscript has been submitted for publication; and after review, a revised version is now under consideration by reviewers: Yao HY, Veine DM, and Livant DL (2015) Therapeutic Inhibition of Breast Cancer Bone Metastasis Progression and Lung Colonization: Breaking the Vicious Cycle by Targeting α5β1 Integrin.

CONCLUSION: The PhScN peptide is a highly potent inhibitor of α5β1 integrin–mediated, serum–induced invasion because it suppresses covalent, disulfide bond formation with its target. Moreover, results of competition assays show that it targets the same region of α5β1 integrin as the PHSCN peptide parent.

REFERENCES:

1. Donate, F., G.C. Parry, Y. Shaked, H. Hensley, et al., *Pharmacology of the novel antiangiogenic peptide ATN-161 (Ac-PHSCN-NH2): Observation of a U-shaped dose-response curve in several preclinical models of angiogenesis and tumor growth.* Clin Cancer Res, 2008. **14**: p. 2137-2144. PMID: 18381955
2. Takada, Y., X. Ye, and S. Simon, *The integrins.* Genome Biol, 2007. **8**(5): p. 215. PMID: 17543136
3. Jia, Y., Z.Z. Zeng, S.M. Markwart, K.F. Rockwood, et al., *Integrin fibronectin receptors in matrix metalloproteinase-1-dependent invasion by breast cancer and mammary epithelial cells.* Cancer Res, 2004. **64**(23): p. 8674-81. PMID: 15574776
4. Livant, D.L., R.K. Brabec, K.J. Pienta, D.L. Allen, et al., *Anti-invasive, antitumorigenic, and antimetastatic activities of the PHSCN sequence in prostate carcinoma.* Cancer Res, 2000. **60**(2): p. 309-320. PMID: 10667582
5. Zeng, Z.-Z., H. Yao, E.D. Staszewski, K.F. Rockwood, et al., *(alpha)5(beta)1 integrin ligand PHSRN induces invasion and (alpha)5 mRNA in endothelial cells to stimulate angiogenesis.* Transl Oncol., 2009. **2**: p. 8-20. PMID: 19252747
6. Clevers, H., *At the crossroads of inflammation and cancer.* Cell, 2004. **118**(6): p. 671-4. PMID: 15369667
7. Coussens, L.M. and Z. Werb, *Inflammation and cancer.* Nature, 2002. **420**(6917): p. 860-7. PMID: 12490959
8. Scherer, R.L., J.O. McIntyre, and L.M. Matrisian, *Imaging matrix metalloproteinases in cancer.* Cancer Metastasis Rev, 2008. **27**(4): p. 679-90. PMID: 18465089
9. Livant, D.L., R.K. Brabec, K. Kurachi, D.L. Allen, et al., *The PHSRN sequence induces extracellular matrix invasion and accelerates wound healing in obese diabetic mice.* J Clin Invest, 2000. **105**(11): p. 1537-1545. PMID: 10841512
10. Zeng, Z.-Z., Y.F. Jia, N.J. Hahn, S.M. Markwart, et al., *Role of focal adhesion kinase and phosphatidylinositol 3'-kinase in integrin fibronectin receptor-mediated, matrix metalloproteinase-1 dependent invasion by metastatic prostate cancer cells.* Cancer Res, 2006. **66**(16): p. 8091-8099. PMID: 16912186
11. van Golen, K.L., L. Bao, G.J. Brewer, K.J. Pienta, et al., *Suppression of tumor recurrence and metastasis by a combination of the PHSCN sequence and the antiangiogenic compound tetrathiomolybdate in prostate carcinoma.* Neoplasia, 2002. **4**(5): p. 373-9. PMID: 12192595
12. Yao, H., D. Veine, K. Fay, E. Staszewski, et al., *The PHSCN dendrimer as a more potent inhibitor of human breast cancer cell invasion, extravasation, and lung colony formation.* Breast Cancer Research and Treatment, 2011. **125**: p. 363-375. PMID: 20300829
13. Yao, H., D.M. Veine, Z.Z. Zeng, K.S. Fay, et al., *Increased potency of the PHSCN dendrimer as an inhibitor of human prostate cancer cell invasion, extravasation, and lung colony formation.* Clin Exp Metastasis, 2010. **27**(3): p. 173-84. PMID: 20339907
14. Woods Ignatoski, K.M., N.K. Grewal, S. Markwart, D.L. Livant, and S.P. Ethier, *p38MAPK induces cell surface alpha4 integrin downregulation to facilitate erbB-2-mediated invasion.* Neoplasia, 2003. **5**(2): p. 128-34. PMID: 12659685

15. Woods Ignatoski, K.M., D.L. Livant, S. Markwart, N.K. Grewal, and S.P. Ethier, *The role of phosphatidylinositol 3'-kinase and its downstream signals in erbB-2-mediated transformation.* Mol Cancer Res, 2003. **1**(7): p. 551-60. PMID: 12754302
16. Aota S, Nomizu M, Yamada KM (1994) The short amino acid sequence Pro-His-Ser-Arg-Asn in human fibronectin enhances cell-adhesive function. J Biol Chem 269 (40):24756-24761
17. Veine DM, Yao H, Stagfford DR, Fay KS, Livant DL (2014) A D–amino acid containing peptide as a potent, noncovalent inhibitor of alpha5beta1 integrin in human prostate cancer invasion and lung colonization. Clin. Exp. Metastasis. doi:10.1007/s10585-013-9634-1.
18. Motulsky HJ, Neubig RR (2010) Analyzing binding data. Current protocols in neuroscience / editorial board, Jacqueline N Crawley [et al] Chapter 7:Unit 7 5. doi:10.1002/0471142301.ns0705s52
19. van Golen KL, Bao L, Brewer GJ, Pienta KJ, Kamradt JM, Livant DL, Merajver SD (2002) Suppression of tumor recurrence and metastasis by a combination of the PHSCN sequence and the antiangiogenic compound tetrathiomolybdate in prostate carcinoma. Neoplasia 4 (5):373-379. doi:10.1038/sj.neo.7900258 [doi]
20. Khalili P, Arakelian A, Chen G, Plunkett ML, Beck I, Parry GC, Donate F, Shaw DE, Mazar AP, Rabbani SA (2006) A non-RGD-based integrin binding peptide (ATN-161) blocks breast cancer growth and metastasis in vivo. Mol Can Ther 5:2271-2280
21. Stoeltzing O, Liu W, Reinmuth N, Fan F, Parry GC, Parikh AA, McCarty MF, Bucana CD, Mazar AP, Ellis LM (2003) Inhibition of integrin alpha5beta1 function with a small peptide (ATN-161) plus continuous 5-FU infusion reduces colorectal liver metastases and improves survival in mice. Int J Cancer 104:496-503
22. Zeng Z-Z, Jia YF, Hahn NJ, Markwart SM, Rockwood KF, Livant DL (2006) Role of focal adhesion kinase and phosphatidylinositol 3'-kinase in integrin fibronectin receptor-mediated, matrix metalloproteinase-1 dependent invasion by metastatic prostate cancer cells. Cancer Res 66 (16):8091-8099
23. Cianfrocca ME, Kimmel KA, Gallo J, Cardoso T, Brown MM, Hudes G, Lewis N, Weiner L, Lam GN, Brown SC, Shaw DE, Mazar AP, Cohen RB (2006) Phase 1 trial of the antiangiogenic peptide ATN-161 (Ac-PHSCN-NH(2)), a beta integrin antagonist, in patients with solid tumours. Br J Cancer 94 (11):1621-1626. doi:6603171 [pii] 10.1038/sj.bjc.6603171
24. Gupta GP, Massague J (2006) Cancer metastasis: building a framework. Cell 127 (4):679-695. doi:10.1016/j.cell.2006.11.001
25. Jean C, Gravelle P, Fournie JJ, Laurent G (2011) Influence of stress on extracellular matrix and integrin biology. Oncogene 30 (24):2697-2706. doi:10.1038/onc.2011.27
26. Husemann Y, Geigl JB, Schubert F, Musiani P, Meyer M, Burghart E, Forni G, Eils R, Fehm T, Riethmuller G, Klein CA (2008) Systemic spread is an early step in breast cancer. Cancer cell 13 (1):58-68. doi:10.1016/j.ccr.2007.12.003
27. Mundy GR (2002) Metastasis to bone: causes, consequences and therapeutic opportunities. Nat Rev Cancer 2 (8):584-593. doi:10.1038/nrc867
28. Suva LJ, Winslow GA, Wettenhall RE, Hammonds RG, Moseley JM, Diefenbach-Jagger H, Rodda CP, Kemp BE, Rodriguez H, Chen EY, et al. (1987) A parathyroid hormone-related protein implicated in malignant hypercalcemia: cloning and expression. Science 237 (4817):893-896
29. Esbrit P, Alvarez-Arroyo MV, De Miguel F, Martin O, Martinez ME, Caramelo C (2000) C-terminal parathyroid hormone-related protein increases vascular endothelial growth factor in human osteoblastic cells. Journal of the American Society of Nephrology : JASN 11 (6):1085-1092
30. Alonso V, de Gortazar AR, Ardura JA, Andrade-Zapata I, Alvarez-Arroyo MV, Esbrit P (2008) Parathyroid hormone-related protein (107-139) increases human osteoblastic cell survival by activation of vascular endothelial growth factor receptor-2. J Cell Physiol 217 (3):717-727. doi:10.1002/jcp.21547

31. Isowa S, Shimo T, Ibaragi S, Kurio N, Okui T, Matsubara K, Hassan NM, Kishimoto K, Sasaki A (2010) PTHrP regulates angiogenesis and bone resorption via VEGF expression. Anticancer research 30 (7):2755-2767
32. Guise TA (1997) Parathyroid hormone-related protein and bone metastases. Cancer 80 (8 Suppl):1572-1580
33. Kong YY, Yoshida H, Sarosi I, Tan HL, Timms E, Capparelli C, Morony S, Oliveira-dos-Santos AJ, Van G, Itie A, Khoo W, Wakeham A, Dunstan CR, Lacey DL, Mak TW, Boyle WJ, Penninger JM (1999) OPGL is a key regulator of osteoclastogenesis, lymphocyte development and lymph-node organogenesis. Nature 397 (6717):315-323. doi:10.1038/16852
34. Blair HC, Teitelbaum SL, Ghiselli R, Gluck S (1989) Osteoclastic bone resorption by a polarized vacuolar proton pump. Science 245 (4920):855-857
35. Delaisse JM, Engsig MT, Everts V, del Carmen Ovejero M, Ferreras M, Lund L, Vu TH, Werb Z, Winding B, Lochter A, Karsdal MA, Troen T, Kirkegaard T, Lenhard T, Heegaard AM, Neff L, Baron R, Foged NT (2000) Proteinases in bone resorption: obvious and less obvious roles. Clinica chimica acta; international journal of clinical chemistry 291 (2):223-234
36 Tang X, Zhang Q, Shi S, Yen Y, Li X, Zhang Y, Zhou K, Le AD (2010) Bisphosphonates suppress insulin-like growth factor 1-induced angiogenesis via the HIF-1alpha/VEGF signaling pathways in human breast cancer cells. Int J Cancer 126 (1):90-103. doi:10.1002/ijc.24710
37. Peoples GE, Blotnick S, Takahashi K, Freeman MR, Klagsbrun M, Eberlein TJ (1995) T lymphocytes that infiltrate tumors and atherosclerotic plaques produce heparin-binding epidermal growth factor-like growth factor and basic fibroblast growth factor: a potential pathologic role. Proceedings of the National Academy of Sciences of the United States of America 92 (14):6547-6551
38. Petersen M, Pardali E, van der Horst G, Cheung H, van den Hoogen C, van der Pluijm G, Ten Dijke P (2010) Smad2 and Smad3 have opposing roles in breast cancer bone metastasis by differentially affecting tumor angiogenesis. Oncogene 29 (9):1351-1361. doi:10.1038/onc.2009.426
39. Winding B, Misander H, Sveigaard C, Therkildsen B, Jakobsen M, Overgaard T, Oursler MJ, Foged NT (2000) Human breast cancer cells induced angiogenesis, recruitment, and activation of osteoclasts in osteolytic metastasis. Journal of cancer research and clinical oncology 126 (11):631-640
40. Van der Velde-Zimmermann D, Verdaasdonk MA, Rademakers LH, De Weger RA, Van den Tweel JG, Joling P (1997) Fibronectin distribution in human bone marrow stroma: matrix assembly and tumor cell adhesion via alpha5 beta1 integrin. Exp Cell Res 230 (1):111-120. doi:S0014-4827(96)93405-9 [pii] 10.1006/excr.1996.3405
41. Noguchi M, Morioka E, Ohno Y, Noguchi M, Nakano Y, Kosaka T (2013) The changing role of axillary lymph node dissection for breast cancer. Breast cancer 20 (1):41-46. doi:10.1007/s12282-012-0416-4
42. Dickson RB, Lippman ME (2001) Cancer of the Breast. In: DeVita VT, Hellman S, Rosenberg SA (eds) Cancer: Principles & Practice of Oncology. 6th edn. Lippencott Williams & Wilkins, Philadelphia, pp 1633-1726
43. Anderson JA, Grabowska AM, Watson SA (2007) PTHrP increases transcriptional activity of the integrin subunit alpha5. Br J Cancer 96 (9):1394-1403. doi:10.1038/sj.bjc.6603720
44. Yao H, Zeng Z-Z, Fay KS, Veine DM, Straszewski ED, Morgan MA, Wilder-Romans K, Williams TM, Spalding AC, Ben-Josef E, Livant DL (2011b) Role of alpha5beta1 integrin upregulation in radiation-induced invasion by human pancreatic cancer cells. Transl Oncol 4 (5):282-292
45. Livant DL, Brabec RK, Kurachi K, Allen DL, Wu Y, Andrews P, Ethier SP, Markwart S (2000) The PHSRN sequence induces extracellular matrix invasion and accelerates wound healing in obese diabetic mice. J Clin Invest 105 (11):1537-1545

46. Boire A, Covic L, Agarwal A, Jacques S, Sherifi S, Kuliopulos A (2005) PAR1 is a matrix metalloprotease-1 receptor that promotes invasion and tumorigenesis of breast cancer cells. Cell 120 (3):303-313. doi:10.1016/j.cell.2004.12.018
47. Blackburn JS, Brinckerhoff CE (2008) Matrix metalloproteinase-1 and thrombin differentially activate gene expression in endothelial cells via PAR-1 and promote angiogenesis. The American journal of pathology 173 (6):1736-1746. doi:10.2353/ajpath.2008.080512
48. Foley J, Nickerson N, Riese DJ, 2nd, Hollenhorst PC, Lorch G, Foley AM (2012) At the crossroads: EGFR and PTHrP signaling in cancer-mediated diseases of bone. Odontology / the Society of the Nippon Dental University 100 (2):109-129. doi:10.1007/s10266-012-0070-5
49. Ignatoski KM, Maehama T, Markwart SM, Dixon JE, Livant DL, Ethier SP (2000) ERBB-2 overexpression confers PI 3' kinase-dependent invasion capacity on human mammary epithelial cells. Br J Cancer 82 (3):666-674. doi:S0007092099909795 [pii] 10.1054/bjoc.1999.0979
50. Woods IKM, Grewal NK, Markwart SM, Livant DL, Ethier SP: p38MAPK induces cell surface alpha4 integrin down regulation to facilitate erbB2-mediated invasion. Neoplasia 5(2): 128-34, 2003. PM12659685/PMCID: PMC1550346